Yanqiu Zhao*, Lunwei Wang, Leander Siegle, and Harald Giessen

Lateral shear interferometry for shape accuracy measurements of 3D-printed micro-optics

https://doi.org/10.1515/cdbme-2024-2170

Abstract: The technique of 3D-printed micro-optics has experienced significant advancements over the last few years [1, 2]. This progressive evolution has been marked by remarkable strides in precision and miniaturization, making it particularly attractive to applications in the field of medical endoscopy. One noteworthy application entails the fabrication of micro-lenses directly on optical fibers, thereby creating endoscopic devices with unparalleled capabilities. A significant attribute of these micro-optical systems lies in their capability for precise imaging and their adept navigation through exceptionally narrow biological structures. For instance, the application of the 3D-printed endoscopy technology has facilitated insertion into the aorta of mice, as well as severely diseased human carotid arteries [2, 3]. This unprecedented level of accessibility and adaptability holds immense promise for diagnostic and therapeutic interventions in the realm of cardiovascular medicine and beyond. In the future, it may also be conceivable for micro-lenses to serve not only as imaging tools, but also as integral components of 3D-printing processes aimed at repairing damaged human tissue with bio-materials.

For micro-lens production and quality control, performance assessment is invariably necessary to assure diffraction-limited imaging in the different optical applications. With confocal surface profiling, only the surface shape information of micro-optics can be obtained. However, not only the shape of 3D-printed optics is relevant for its quality, but also its refractive index distribution is crucial when determining its overall optical performance. Therefore, the measurement of the wavefront is decisive in evaluating lens performance. Lateral shear interferometry presents itself as a compact and precise method for wavefront measurements. The only essential component required in the set-up is a pair of glass plates with high surface quality. Consequently, the entire set-up can be notably streamlined, as there is no requirement to construct an interferometer reference arm. This advantage facilitates the development of a notably compact set-up, making lateral shear interferometry particularly advantageous for integration with microscope and 3D-printer, despite the requirement for more complex algorithms in analyzing lateral shear interferograms.

In this paper, simulation of shear interferogram fringes corresponding to wavefronts exhibiting varying aberrations are discussed. Additionally, this research encompasses measurement and analysis of shear interferograms obtained from wavefronts transmitted through different lenses. Through meticulous examination of these experimental results, the characteristics and performance of the tested optical systems are elucidated, contributing to a deeper understanding of wavefront analysis methodologies and their applicability in optical characterization studies.

Keywords: 3D-printed micro-optics, 3D-printed endoscopy technology, shear interferometry, wavefront measurement, shape accuracy measurement

1 Theoretical background

1.1 Lateral shear plate interferometer

Unlike conventional interferometers such as a Michelson interferometer and a Mach-Zender interferometer, where the testing beam overlaps with a reference beam that has plane wavefronts, a lateral shear superimposes the replicas of itself. In the overlapping area of two reflected beams, fringes can be observed. The interferogram fringes carry comprehensive information regarding the wavefront being tested. Through the analysis of both bright and dark fringes, optical path differences can be calculated, thus wavefront information is acquired. The optical path difference for a shear plate set-up is calculated as:

$$OPD = W(x+S,y) - W(x,y) = \frac{\partial W(x,y)}{\partial x} \cdot S = m\lambda \quad (1)$$

with wavefront W and shear distance S. When the shear distance is very small, the optical path difference (OPD) can be approximated as the product of the derivative of the wavefront and the shear distance[4]. When, the OPD equals an integer multiple of the wavelength, the condition for bright fringes is fulfilled.

***Corresponding author: Yanqiu Zhao,** 4th Physics Institute, University of Stuttgart, Pfaffenwaldring 57, Stuttgart, Germany, e-mail: yanqiu.zhao@pi4.uni-stuttgart.de

Lunwei Wang, Leander Siegle, Harald Giessen, Institution (4th Physics Institute, University of Stuttgart, Stuttgart, Germany

For a shear plate interferometer, only a simple glass plate with high surface quality is required to provide two reflected beams with a certain shear distance, as shown in Figure 1.

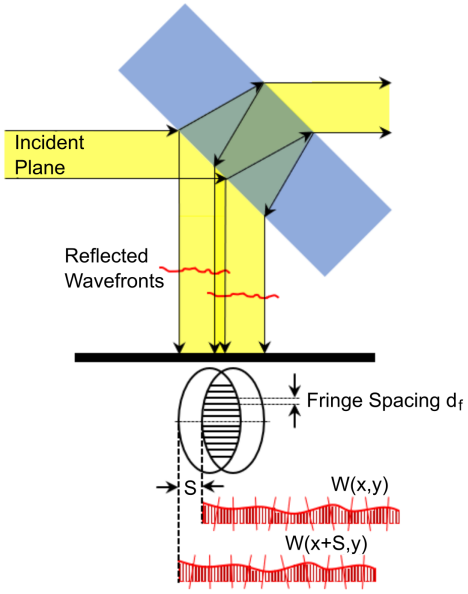

Fig. 1: Shear plate interferometer.

1.2 Wavefront errors on shear interferogram

Generated by a reference beam with a perfect plane wavefront and the testing beam, conventional interferograms represent the wavefront shape directly. In contrast, shear interferograms depict the wavefront derivative: the fringes on shear interferograms show constant local slope of the tested wavefront, thereby serving as crucial indicators for wavefront analysis [5], akin to a "height map" of the wavefront derivative. Altering the shear distance and the slight wedge angle of the glass plate modifies the position and orientation of the wavefront derivative, consequently yielding varied fringe distances and even patterns.

2 Experimental set-up

In the realm of this paper, a single lateral shear interferometer is built to measure the testing micro-lenses. In this set-up, the wavefront measurement becomes accurate, easy and as compact as possible. The micro-lenses are printed using a Nanoscribe Quantum X two-photon 3D printer and photoresist IP-S on glass substrates [6].

2.1 Air-wedge shear-plate interferometer set-up

In the shear plate interferometer set-up, a pair of glass shear plates serves as the amplitude separator instead of the double frequency grating that is used in a Ronchi grating set-up. These shear glass plates, crafted from fused silica, have a diameter of 50.8 mm and a surface flatness of $\lambda/20$. They are meticulously mounted on two mirror mounts and interconnected through three distance adjusters, as demonstrated in Figure 2. This design facilitates rotational adjustment in two directions for one of the glass plates, thereby enabling alterations to the wedge angle of the air slit along two axes and the distance between the two glass plates without inducing beam deviation from the optical axis [7].

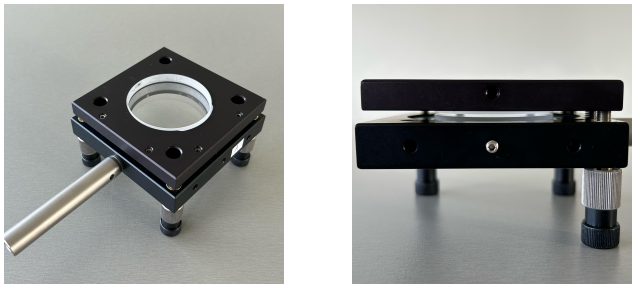

Fig. 2: Air-wedge shear-plate pair in the set-up, inspired by [7].

As depicted in Figure 3, a He-Ne laser with 623.8 nm wavelength and 5 mW intensity traverses firstly through a Nikon M42 zoom objective with a focal length ranging from 80 mm to 200 mm. This objective facilitates the full illumination of micro-lenses present on the substrate by introducing a slight convergence to the light beam and by precisely adjusting the position of the micro-lenses under examination. Subsequently, the laser beam pass through the micro-lenses under examination and is then re-collimated by a microscope objective. The set of microscope objectives utilized comprises lenses with specifications of 20X/ NA 0.45 and 50X/ NA 0.55. Following re-collimation, the laser beam encounters a pair of optical flats positioned at a 45-degree angle to the optical axis and is reflected by a flat mirror before the interferogram is captured by a camera. The incident light beam undergoes four reflections by both sides of the two optical flats. Nonetheless, the recording process exclusively captures the reflections occurring at the inner sides of the glass plate pair, as detailed in Figure 3. This selective recording is due to the adjustability of the shear between the two beams, facilitated by modifications to the air slit wedge angle and the spacing between the two glass plates. Hence, the irises are adjusted permit only the per-

tinent reflections to pass through. Within this set-up, different micro-lenses are tested via manipulation of the substrate using a 3D stage, and the resulting interferograms are recorded for subsequent analysis.

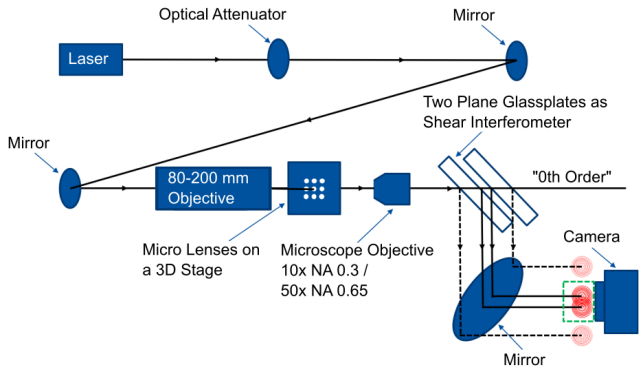

Fig. 3: Shear plate interferometer set-up.

Figure 4 provides a visual representation of the actual set-up.

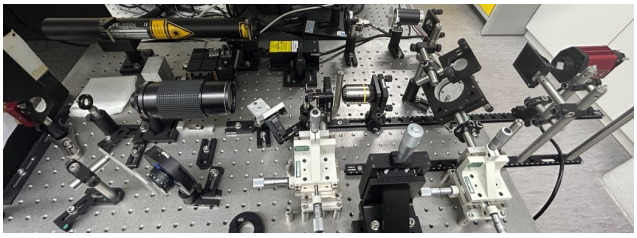

Fig. 4: Photo of the shear plate interferometer set-up.

The cameras used to capture the interferogram are Prosilica GT 6400 mono from Allied Vision with a resolution of 6480 (H) · 4860 (V) and a pixel size 3.45 μm · 3.45 μm. Alternatively, a colour CMOS camera is incorporated into the set-up to capture chromatic interferogram photos. This camera offers a resolution of 4096 (H) · 3000 (V) and a pixel size of 3.45 μm · 3.45 μm.

3 Result and discussion

In the sample presented, lenses designed intentionally with coma, astigmatism, and spherical aberration are fabricated using the Nanoscribe Quantum X printer on a glass substrate. For each type of aberration, the levels of aberration, from left to right, are 0.0 λ (only for spherical aberration), 0.3 λ, 0.5 λ, 0.7 λ, 1.0 λ, 1.3 λ, 1.5 λ and 2.0 λ. Each aberration series is printed three times, maintaining consistent design parameters, see Figure 5. The lenses are fabricated using photoresist IP-S and have a diameter of 140 μm, utilizing two-photon gray scale lithography.

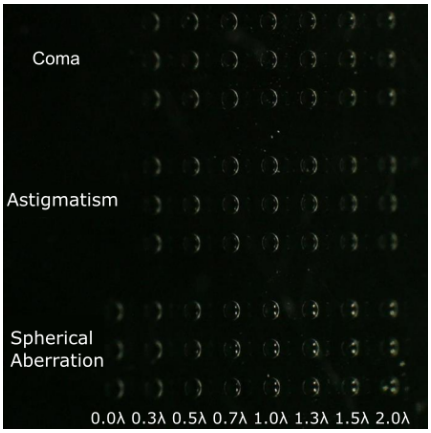

Fig. 5: Microscope photo of 3D-printed micro-lenses with different deliberately designed aberration with oblique illumination.

In the first row of Figure 6, the contour lines of x-direction derivative of a spherically aberrated wavefront are projected onto the X-Y plane. These contour lines correspond to the shear interferogram fringes of lenses with spherical aberration. As the level of spherical aberration increases from left to right (0.0 λ, 0.5 λ, 1.0 λ, and 2.0 λ), the characteristic two-eye pattern becomes more pronounced, and the two eyes progressively move closer to the center. The second row of Figure 6 presents experimental shear interferogram fringes for lenses with varying levels of spherical aberration (0.0 λ, 0.5 λ, 1.0 λ, and 2.0 λ). In the third row, the simulated intensity maps of two identical overlapping beams, each subjected to the corresponding level of spherical aberration, are displayed. When comparing the mathematical model illustrated in the first row, the experimental shear interferograms in the second row, and the simulated intensity maps in the third row, it is evident that they all exhibit similar fringe patterns. Furthermore, as the level of aberration increases, the fringe patterns display analogous trends in their changes. This observation substantiates the efficacy of our method in determining Seidel aberrations in 3D-printed micro-optics.

Figure 7 shows the same analytical method as Figure 6 but for lenses with varying levels of coma aberration (0.0 λ, 0.5 λ, 1.0 λ, and 2.0 λ). Across all three methods, the shear interferogram fringes display segments of concentric rings, mirroring the projected contour lines of the x-direction derivative of a wavefront with x-coma aberration. Additionally, as the level

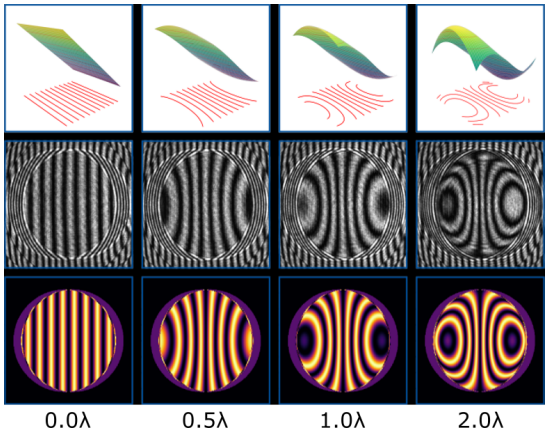

Fig. 6: Lenses with different spherical aberration. First row: wavefront spatial derivative ∂ W / ∂ x and its constant height lines below; Second row: measured shear-plate interferograms; Third row: simulated lateral shear interferograms assuming the designed aberrations. The numbers below give the RMS aberration.

of coma aberration increases, the radius of curvature of the interferogram fringes decreases accordingly.

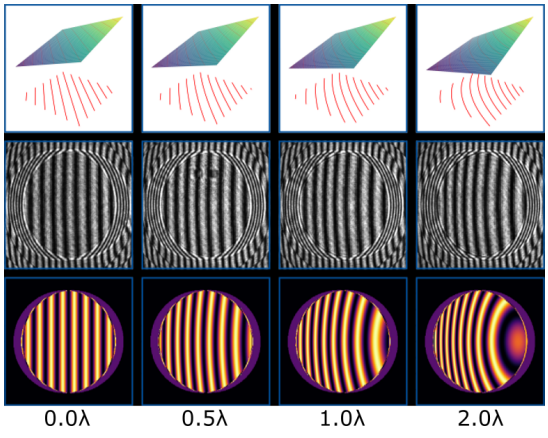

Fig. 7: Lenses with different coma aberration. First row: wavefront spatial derivative ∂ W / ∂ x and its constant height lines below; Second row: measured shear-plate interferograms; Third row: simulated lateral shear interferograms assuming the designed aberrations. The numbers below give the RMS aberration.

The shear interferometer method and results should be compared with previous studies [8, 9], which utilized significantly more complex interferometric set-ups, such as Twyman-Green, Mach-Zehnder, or Michelson interferometers, to achieve sub-wavelength accuracy in surface shape measurements. In contrast, the shear interferometric set-up is considerably simpler to install and exhibits greater resistance to vibrations, yet easily resolving deep sub-wavelength aberration of the 3D-printed microlenses.

4 Conclusion

By analyzing the mathematical models, experimental interferogram fringes and simulated intensity maps, we have demonstrated that our approach accurately captures the effects of spherical aberration and coma aberration on the wavefront and resulting interferogram fringes. The consistent patterns across theoretical, experimental, and simulated data confirm the reliability of our technique in characterizing aberrations in micro-optical elements produced via 3D printing technology. This validation is crucial for advancing the precision and application of 3D-printed optical components in various scientific and industrial fields.

Moreover, shear interferometry provides a direct, rapid and dependable method for measuring wavefronts on 3D-printed micro-optics. Its compact design facilitates easy integration into microscope set-ups. Furthermore, there are prospective plans to integrating the shear plate interferometer directly into the 3D printer. This integration aims to enable real-time optimization of optics printing alongside the printing process itself.

Author Statement

Research funding: ERC PoC 3DPrintedOptics, EU Pathfinder 3DPrint2Market, IEC. DFG GRK2642, BMBF Integrated3DPrint, QR.X, Zeiss Stiftung Endoprint3D, EU Horizon IEC “IV-Lab“: 101115545.

References

[1] T. Gissibl, S. Thiele and A. Herkommer. Nature Photon **10**, 554–560 (2016).
[2] J. Li et al., Light: Science & Applications **9**, 124 (2020).
[3] J. Li et al., Small **18**, 2107032 (2022).
[4] Daniel Malacara, Manuel Servín, and Zacarias Malacara, “Interferogram Analysis For Optical Testing“ Second Edition, Boca Raton, 2005.
[5] Eric P. Goodwin and James C. Wyant, “Field Guide to Interferometric Optical Testing“, Washington, 2006.
[6] S. Thiele, K. Arzenbacher, T. Gissibl, H. Giessen, and A. M. Herkommer, Sci. Adv. **3 (2)**, e1602655. (2017).
[7] G.S.Sarkisov, Instruments and Experimental Techniques **39**, No. 5. 727-731 (1996).
[8] Stephan Reichelt, Alexander Bieber, Bernd Aatz, and Hans Zappe, Proc. SPIE. **5856**, Optical Measurement Systems for Industrial Inspection IV (2005).
[9] Peter de Groot, Adv. Opt. Photon. **7**, 1-65 (2015).